

1 Investigating uncharacterised genes in *Saccharomyces* 2 *cerevisiae* using Robot Scientists

3 Erik Y. Bjurström (erikbju@chalmers.se)¹, Alexander H. Gower (gower@chalmers.se)²,
4 Praphapan Lasin (b.p.lasin@gmail.com)¹, Otto I. Savolainen (otto.savolainen@chalmers.se)^{1,3},
5 Ievgeniia A. Tiukova (tiukova@chalmers.se)^{1,4}, Ross D. King (rossk@chalmers.se)^{1,2,5,6}

6 1. Department of Life Sciences, Chalmers University of Technology, Göteborg, Sweden

7 2. Department of Computer Science and Engineering, Chalmers University of Technology, Göteborg, Sweden

8 3. Department of Clinical Nutrition, University of Eastern Finland, Kuopio, Finland

9 4. Division of Industrial Biotechnology, KTH Royal University of Technology, Stockholm, Sweden

10 5. Department of Chemical Engineering and Biotechnology, University of Cambridge, Cambridge, UK

11 6. Alan Turing Institute, London, UK

12 Abstract

13 Despite extensive research on *Saccharomyces cerevisiae* functional genomics,
14 approximately 880 out of ~6,000 open reading frames (ORFs) remain uncharacterised.
15 In this study we propose a method for characterising genes with limited prior functional
16 knowledge using an automated laboratory platform, in conjunction with several
17 hypothesis instantiation methods. We demonstrate this method by investigating
18 *YGR067C*, an uncharacterised ORF hypothesised to regulate respiration during the
19 diauxic shift. Predictions of the first-order effects of deletion were obtained by curating
20 a list of pathways relevant to the hypothesis. Higher-order effects were predicted using
21 simulation models based on the GEM Yeast9. The predictions were tested using
22 empirical data from biological experiments performed in the Robot Scientist Eve, which
23 generated OD₅₆₀, transcriptomics, and metabolomics data.

24 We observed that *YGR067C* deletion led to downregulation of transcripts in some
25 ethanol consuming respiratory pathways during the glucose phase. During the ethanol
26 phase we observed that NAD⁺, NADP⁺ and NADH accumulated, and several amino acid
27 biosynthesis pathways were enriched for the *ygr067cΔ* strain, suggesting longer term
28 consequences of *YGR067C* mediated regulation. Based on these observations we
29 propose that the role of *YGR067C* during the diauxic shift is to regulate genes related to
30 ethanol consumption and respiration in the glucose phase.

31

32 **Introduction**

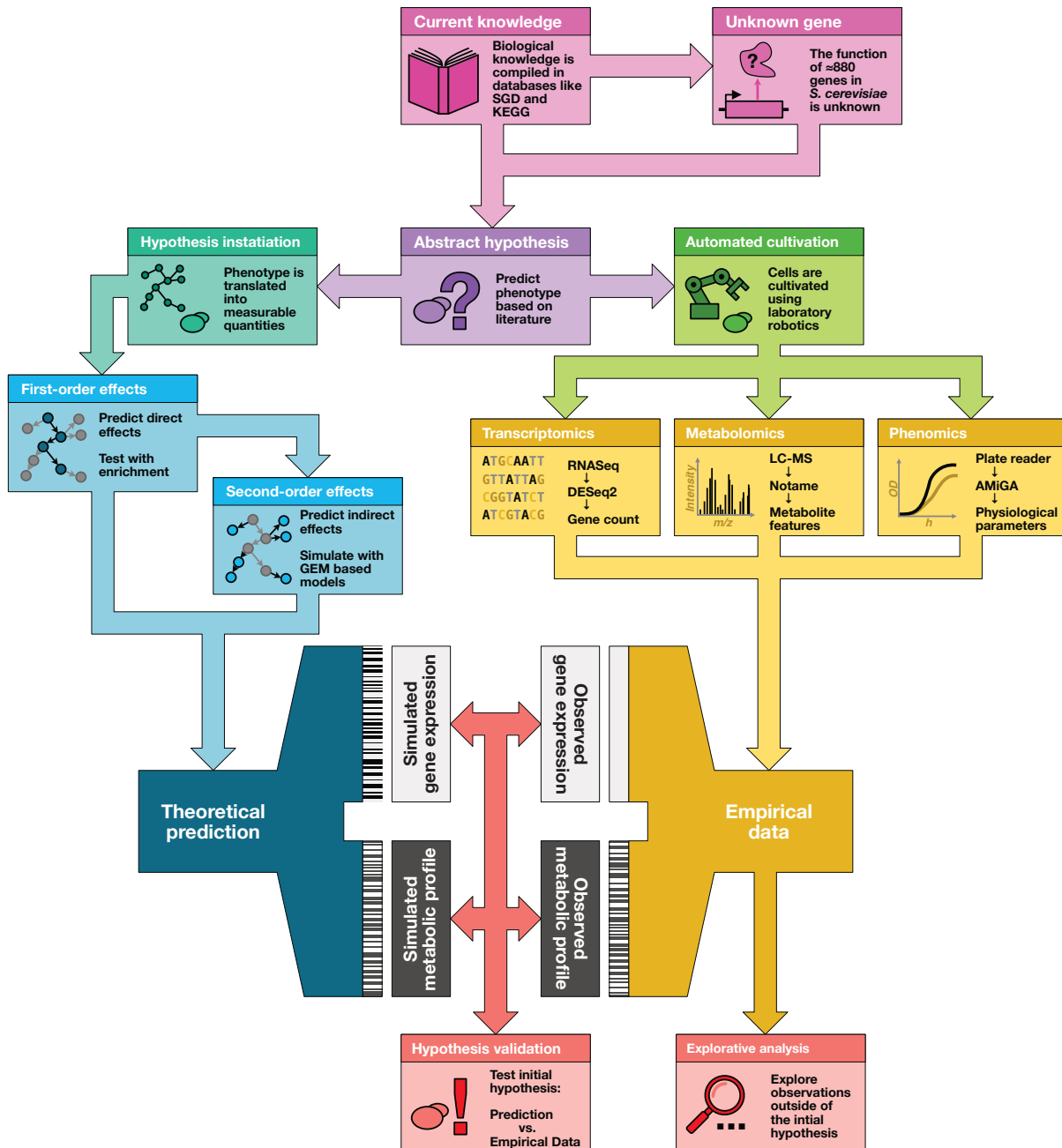
33 *Saccharomyces cerevisiae* is the most studied eukaryotic model organism. Despite
34 this, there are many genes whose biological function is not understood, and a complete
35 understanding of the yeast cell is still far from being achieved¹. The rate at which we
36 progress toward this goal is limited by human capacity for experimentation and
37 experiment design. To increase the effectiveness of systems biology, we can use
38 computational techniques to select or refine hypotheses in a way to maximise
39 information gain, while minimising the time and economic costs, and we can use
40 laboratory automation to increase the quality of empirical data. These are both
41 important aspects for the wider goal of closed-loop automation of functional genomics.
42 In this study we test and compare computational techniques for refining abstract
43 hypotheses, applying them to investigate the biological role of an uncharacterised open
44 reading frame (ORF) in *S. cerevisiae*.

45 When investigating an unknown gene with a hypothesised regulatory function, the first
46 approach would be to identify genes and pathways expected to be directly affected by
47 its deletion. However, we anticipate onward effects across the whole organism from the
48 regulation by the gene of interest, instead of just the immediately affected pathways,
49 metabolites, and genes. To predict these higher-order effects of the knockout we need
50 to perform simulations. And to perform simulations we need a computational model of
51 yeast. There are several computational models available², and which to use depends on
52 several factors, including that we require that inputs and outputs correspond to
53 experimental variables that we can control or measure. We use a flux balance analysis
54 (FBA) model and a first-order logic model, LGEM⁺³. The predictions and simulations are
55 then compared against newly generated empirical data to verify the hypothesis.

56 Obtaining high quality empirical data to test the predictions is complicated by the
57 nature of the hypothesis. Some genes are only active during metabolic transitions, such
58 as the diauxic shift^{4,5}. This necessitates working in dynamical systems, i.e. batch
59 growth, as it would be impossible to observe this effect in stabilised systems such as
60 chemostats⁶. In batch growth, minor fluctuations in initial conditions and sampling time
61 can lead to significant deviations in the empirical data, which complicates statistical
62 inference and affects the reproducibility of the experiment. To address this problem,
63 robot scientists (sometimes “self-driving labs”) have been developed to automate
64 biological experiments to generate highly reproducible scientific results⁷⁻¹⁰. This study
65 used the robot scientist Eve¹¹ to cultivate *S. cerevisiae* and generate multiomics data
66 from a diauxic shift experiment.

67 We investigated the role of *YGR067C*, an uncharacterised ORF whose protein product
68 functionality is unknown. What is known is that the gene product contains a zinc finger
69 motif, similar to that of *Adr1p*, which is a respiratory transcription factor active during
70 the diauxic shift in *S. cerevisiae*^{12,13}. The diauxic shift is a metabolic network rewiring

71 event in *S. cerevisiae*, in which the cell goes from fermentative consumption of glucose
72 and production of ethanol, to respiratory consumption of ethanol once the glucose is
73 depleted¹⁴. During the first growth phase, known as the glucose phase, respiratory
74 genes are repressed by the transcription factor Mig1p¹⁵. As the glucose levels decrease,
75 Mig1p is phosphorylated by Snf1p, relieving the respiratory genes of its repression¹⁵.
76 Adr1p, an activator of respiratory genes such as ADH2, is also activated by Snf1p as the
77 glucose levels decrease¹³. Furthermore, Espinosa et al. observed truncations of
78 YGR067Cp in *S. cerevisiae* strains evolved to assimilate methanol through adaptive
79 laboratory evolution, and suggested that genes and metabolic fluxes that were
80 favourable for growth on methanol were repressed in the presence of a functional
81 YGR067C¹⁶. Thus, based on previous studies⁷ and the structural similarity between
82 YGR067Cp and Adr1p, we hypothesised that YGR067Cp acts as a transcription factor
83 that regulates respiratory genes during the diauxic shift.



84
85 **Figure 1: Instantiation of an abstract hypothesis.** To be able to test a hypothesis, we need to transform it into data
86 that is comparable with empirical data. This instantiation is usually accomplished using a mathematical model; the
87 choice of model, and of the parameters, will change the predictions. To obtain an interface between prediction and
88 measurement where a statistical test can be used, it is most often necessary to transform both the raw model outputs
89 and the raw measurement data. These additional levels of processing risk weakening the signal and amplifying the
90 noise, leading to increased uncertainty in the test, but also enable the opportunity to compare predictions from
91 different models across different measurements.

92 Results

93 We hypothesised that the absence of YGR076C would disrupt respiratory pathways
94 during the diauxic shift in *S. cerevisiae*. To generate the empirical data necessary for
95 testing our hypothesis, a *ygr076cΔ* strain with a reference strain BY4741 was cultivated
96 in the automated laboratory platform Eve. The cells were grown in minimal media with
97 low glucose content (1.25 g/L) to ensure diauxic growth, see Methods section for

98 detailed composition. Glucose phase and ethanol phase samples were taken after 12-
99 and 24-hours post-inoculation, respectively. Transcriptomic samples were obtained
100 using RNAseq (transcriptomics) and metabolomic samples through liquid
101 chromatography-mass spectrometry (LCMS), see Methods section for further details.

102 Pathway set prediction

103 The first order effects of the hypothesised disruption should be observable in the
104 transcription of genes and the metabolism in pathways associated with respiration. A
105 first order prediction was generated by curating a list of genes and metabolites recorded
106 in the Kyoto Encyclopedia of Genes and Genomes (KEGG) database which were
107 associated with respiration, see Methods section. Univariate statistical tests were
108 performed: DESeq2 for transcriptomic data and notame for metabolomic. The
109 hypothesis was then tested on the transcriptomic data using consensus gene set
110 enrichment, which included Fisher's exact test, Boschloo's test, and Fast Gene Set
111 Enrichment Analysis (FGSEA). Individual genes and metabolites within the KEGG
112 pathways were also examined.

113 Transcriptomic analysis indicated that the gene transcription in the tricarboxylic acid
114 (TCA) cycle, oxidative phosphorylation, and glyoxylate pathways were enriched during
115 the glucose phase, see Table 1. Furthermore, FGSEA analysis showed that gene
116 transcription in these pathways was downregulated in the glucose phase, suggesting
117 that transcription is induced by the protein product of *YGR067C* during glucose rich
118 environments. The transcripts of the fermentative glycolysis pathway, pyruvate
119 dehydrogenase complex, and mitochondrial pyruvate importers were not enriched
120 however, see Supplementary Table 4.1. Genes in the gluconeogenesis pathway were
121 statistically enriched during the glucose phase using methods with significance cutoffs
122 (Fisher's and Boschloo's tests) but not FGSEA which considers all genes within a set,
123 see Table 1. The differentially expressed genes (DEGs) within gluconeogenesis pathway,
124 *PYC1* (carboxylase responsible for conversion of pyruvate to oxaloacetate) and *FBP1*
125 (phosphatase responsible for conversion between F1,6BP to F6P), were both
126 downregulated while the genes with an adjusted p-value > 0.05 were upregulated. The
127 transcription of the genes within the predicted pathways were generally downregulated
128 in the deletion mutant during the glucose phase. Only *VMA9* and *VMA10*, both subunits
129 of the H⁺-ATPase complex, were both upregulated and part of the KEGG pathway
130 oxidative phosphorylation (sce00190).

131 **Table 1. Consensus gene set enrichment of respiratory pathways using data from differential gene expression**
 132 **analysis.** Columns describe the statistical test while rows describe phase and pathway. Fisher's test and Boschloo's
 133 test are two-tailed hypothesis tests where genes with a *FDR* < 0.05 were considered significantly differentially
 134 expressed. Only distinct regulation was considered for FGSEA and the directions were split into two separate metrics
 135 (up- and downregulation). Enrichment analysis with a *p*-value < 0.05 were considered statistically significant and are
 136 marked with bold.

		Fisher's test	Boschloo's test	FGSEA up	FGSEA down
Glucose phase	TCA cycle	7.11E-09	5.22E-09	NA	2.22E-03
	Oxidative phosphorylation	4.89E-05	4.27E-09	NA	1.73E-02
	Glyoxylate shunt	3.45E-06	2.38E-06	NA	2.22E-03
	Glycolysis (fermentation)	1	1	NA	7.60E-01
	Glycolysis (respiration)	1	1	NA	1.06E-01
	Gluconeogenesis	4.48E-02	3.94E-02	NA	1.35E-01
Ethanol phase	TCA cycle	1	1	NA	9.03E-02
	Oxidative phosphorylation	1	9.33E-01	NA	2.02E-01
	Glyoxylate shunt	1	8.76E-01	8.72E-01	NA
	Glycolysis (fermentation)	1	1	2.62E-01	NA
	Glycolysis (respiration)	1	1	NA	9.03E-02
	Gluconeogenesis	1	1	8.72E-01	NA

137
 138 Of the 85 metabolites included in first order prediction set, only 14 could be identified in
 139 the empirical data using peak identification software, and of those only 9 passed the
 140 quality control during the pre-processing step, see Supplementary Table 4.1. This was
 141 perhaps not surprising as many of the predicted metabolites are short chain carboxylic
 142 acids, which are known to be difficult to detect in conventional LCMS methods due to
 143 bad reverse phase retention and inefficient electrospray ionisation¹⁷. The abundance of
 144 phosphoenol pyruvate (*p*-value = 0.077, log2-fold change = -0.0805, linear model) and
 145 glutamic acid (*p*-value = 0.078, log2-fold change = 0.87, linear model) were significantly
 146 different in the mutant compared to the reference. During the ethanol phase, increased
 147 accumulation of nicotinamide adenosine dinucleotides could be observed in the
 148 deletion mutant compared to the reference strain: NAD+ (*p*-value = 0.024, log2-fold
 149 change = 2.82, linear model), NADH (*p*-value = 1.9 x 10⁻⁴, log2-fold change = 2.82,

150 linear model), and NADP+ (p-value = 0.039, log2-fold change = 3.96, linear model).
151 While the NADH/NAD+ ratio was unchanged (1.00), an increased NADP+/NAD+ ratio
152 could be observed (1.40). Furthermore, increased accumulation of glutamic acid, which
153 is essential for the anabolism, could be observed (p-value = 0.008, log2-fold change =
154 1.73, linear model) in the ethanol phase.

155

156 Results of the FBA simulation method

157 Using a FBA model with growth as the objective function, we simulated metabolite
158 presence and gene expression for all metabolites and genes in the Yeast9 model, using
159 a pathway perturbation method to instantiate our hypothesis on *YGR067C* function. As
160 FBA does not simulate metabolite accumulation, metabolite presence means that the
161 compound is predicted to be involved in one or more active reactions. Because of the
162 difference in simulation methods, predictions were made for roughly twice as many
163 metabolites as in the LGEM⁺ method, and for roughly three times as many genes,
164 meaning the pathway coverage is greater than either the pathway set prediction method
165 or the LGEM⁺ method, see Table 2.

166 During the glucose phase we predicted that overall, 564 genes would be differentially
167 expressed to some degree in the mutant strain; in the ethanol phase this figure was 554.
168 The pathways predicted to be down-regulated the most during the glucose phase in the
169 mutant were glucose fermentation, pyruvate fermentation, glycolysis, and very long
170 chain fatty acid biosynthesis. In the ethanol phase the pathways predicted by the FBA to
171 be most down-regulated in the mutant were various amino acid and nucleotide
172 biosynthesis pathways, and chorismate metabolism; the pathway predicted most up-
173 regulated was the glyoxylate cycle. In contrast to LGEM⁺, the FBA model predicted that
174 32 and 28 of the detectable metabolites in the glucose and ethanol phases respectively
175 were differentially expressed in the mutant; the model predicted the direction of these
176 differences with an accuracy of 22%.

177 Full tables for the predictions with evaluation against transcriptomics and
178 metabolomics data are provided in the supplementary information, see Supplementary
179 Table 4.2.

180

181 Results of the LGEM⁺ simulation method

182 LGEM⁺ expresses the graph structure of metabolic networks in mathematical logic, then
183 uses an automated theorem prover to simulate (through logical deduction) activated
184 reactions, metabolites, and genes³. Compounds and genes that appear in the LGEM⁺
185 simulation are those predicted to be present. The simulations are not quantitative, so
186 presence is binary, and metabolite presence in the case of LGEM⁺ is defined in the same

187 way as for FBA simulations. We simulated metabolite presence and gene expression for
188 all metabolites and genes in the Yeast9 model, using the same pathway perturbation as
189 the FBA simulations, see Methods section for details on the LGEM⁺ simulations. Most
190 metabolites and genes were predicted not to be present, or expressed, in either the
191 wild-type strain or the YGR067C deletant, see Table 2. Therefore, the predictions were
192 largely that there was no difference between the strains.

193 The LGEM⁺ simulation extends beyond the localised scope of the pathway set
194 prediction, yielding us a prediction of the second-order effect of the hypothesised
195 consequences of YGR067C deletion. During the glucose phase this model predicted 37
196 genes to be differentially expressed in the YGR067C deletant compared to the wild type.
197 Genes involved in glycolysis and pyruvate decarboxylation to acetyl CoA were predicted
198 differentially expressed. Of these, 8 were significantly differentially expressed in the
199 empirical transcriptomic data ($p < 0.05$).

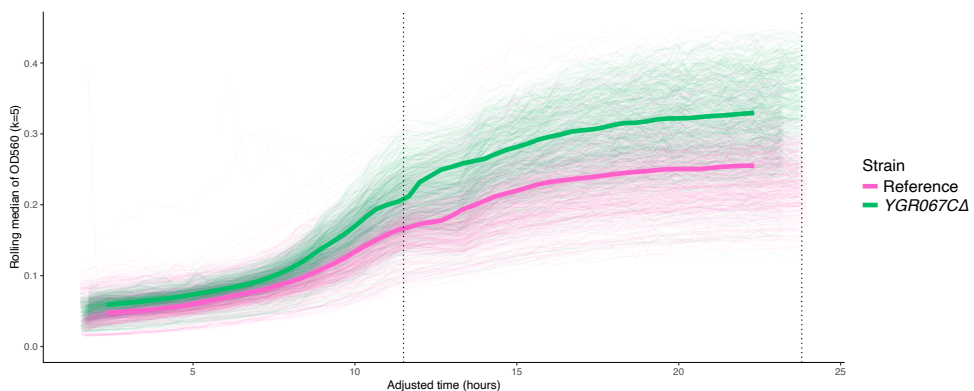
200 Full tables for the predictions with evaluation against transcriptomics and
201 metabolomics data are provided in the supplementary information, see Supplementary
202 Table 4.2.

203
204 *Table 2. Results of simulation methods († - no support for LGEM⁺ metabolomics simulations as there was not
205 overlap between detected metabolites and predicted)*

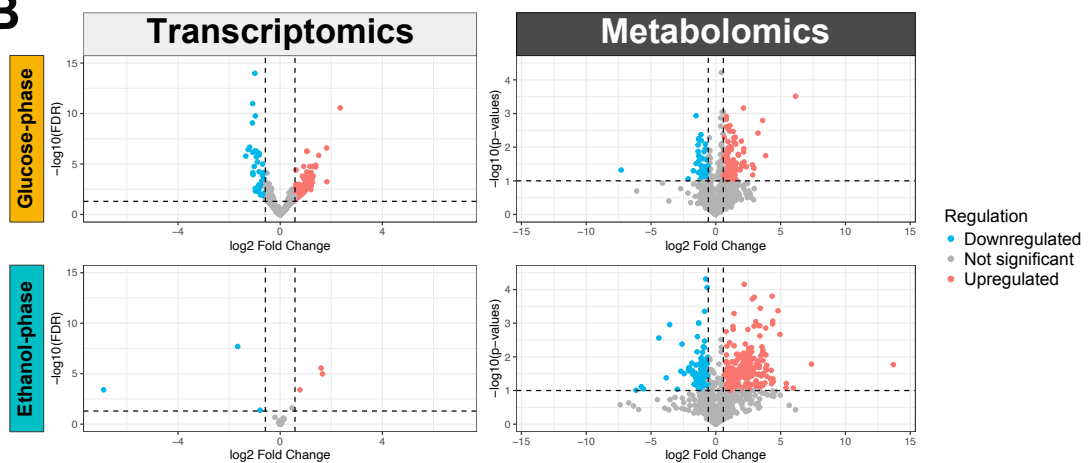
Simulation method	LGEM ⁺		FBA	
Phase	Glucose	Ethanol	Glucose	Ethanol
# Pred. diff expr. genes	37	39	564	554
Direction prediction acc. (genes)	2%	2%	23%	19%
# Pred. diff expr. metabolites	11	18	444	423
Direction prediction acc. (metabolites) [†]	–	–	22%	24%
Predicted affected pathways (in Δ YGR067C)	↑ – ↓ –	↑ pentose phosphate pathway ↓ pyruvate decarboxylation to acetyl CoA	↑ – ↓ glucose fermentation, pyruvate fermentation, glycolysis, very long chain fatty acid biosynthesis	↑ glyoxylate cycle ↓ amino acid and nucleotide biosynthesis

206
207

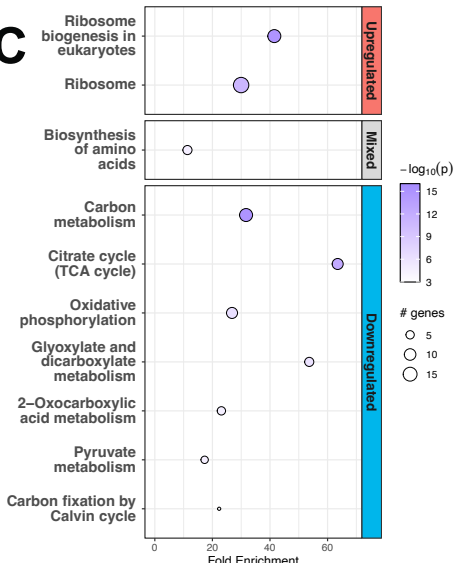
A



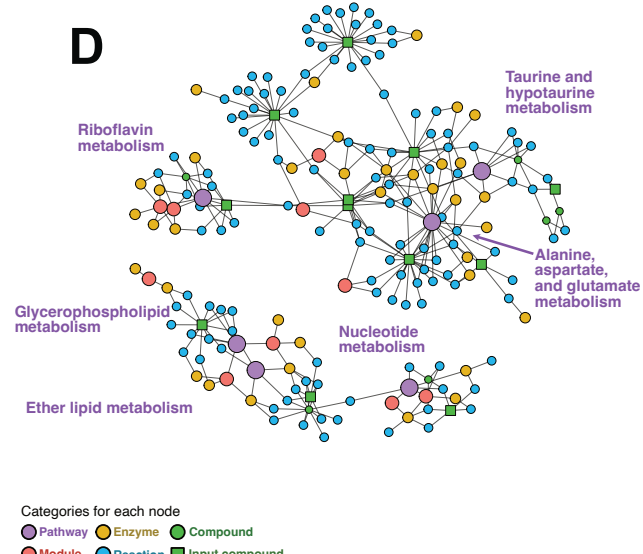
B



C



D



208
209
210
211
212
213
214
215
216
217

Figure 2. **Results outside the initial hypothesis.** A. Averaged growth curves of the *ygr067cΔ* strain (pink) and the reference strain (green) with the 11.5-hour and 24-hour sampling points as a dotted, vertical lines. OD₅₆₀ in the y-axis and time in hours in the x-axis. The bold lines represent a rolling median applied over the measured OD₅₆₀. The thinner lines represent the actual OD₅₆₀ measurements from each replicate. B. Volcano plots representing differential expression of transcriptomics (left column) and metabolomics (right column) during the glucose phase (top row) and the ethanol phase (bottom row). C. Dotplot of pathway enrichment analysis using sub-active networks of the glucose-phase. The top section represents upregulated pathways, middle section mixed regulation, and bottom downregulated pathways. D. Diffusion based topological enrichment using FELLA with significantly enriched pathways in red (FELLA p-score < 0.05).

218 **Results outside the initial hypothesis**

219 Our initial hypothesis was only concerned with a relatively small subset of the recorded
220 data, namely genes and metabolites related to respiration. However, RNAseq and
221 untargeted LCMS attempts to capture the entire transcriptome and metabolome,
222 respectively. Here we present observations regarding the transcriptome and
223 metabolome which was outside of our initial hypothesis. Additionally, since no
224 physiological prediction was made prior to the experiments, this section also covers
225 growth parameters.

226 The *ygr067cΔ* strain grew faster on average and reached a higher OD₅₆₀ at 24 hours
227 compared to the BY4741 reference strain, see Figure 2A. Growth curves were obtained
228 by measuring OD₅₆₀ every 20 minutes with OMEGA Polarstar. The growth curves were
229 then used to estimate physiological parameters (maximum biomass specific growth
230 rate during exponential growth, μ , and carrying capacity, OD_{560, max}). A permutation test,
231 $n = 10,000$, was then performed to compare the growth parameters, see Methods
232 section for detailed explanation. For the reference strain, μ was 0.402 h⁻¹ and 0.450 h⁻¹
233 for the *ygr067cΔ* strain. The $\Delta\mu$ was therefore 0.048 h⁻¹ and the permutation test yielded
234 a p-value = 0.0001. The OD₅₆₀ at 24 hours post-inoculation was 0.265 for the reference
235 strain and 0.338 for the *ygr067cΔ* strain. The mean difference in OD₅₆₀ at 24 hours was
236 thus 0.073 and the permutation test yielded a p-value of 0.0001. The expression of
237 genes responsible for mitochondrial catabolism in the TCA cycle were downregulated in
238 the *ygr067cΔ* mutant, see the subsection on pathway set prediction. The increased
239 biomass yield and biomass specific growth rate in the *ygr067cΔ* mutant could then
240 perhaps be explained by more energy being funnelled into biomass/population growth
241 instead of mitochondrial proteome investment¹⁸. Notably however, the cultures in this
242 study were sampled before ethanol could be depleted. It is therefore unknown if the
243 biomass yield in the *ygr067cΔ* mutant would remain higher than the reference strain
244 post-ethanol depletion.

245 Our data suggest that the activity of *YGR067C*—which is assumed to be a transcription
246 factor—is more pronounced during the fermentative glucose phase, while the
247 metabolic consequences of *YGR067C* mediated regulation can be observed in both
248 glucose- and ethanol phase. The gene deletion affected gene expression during the
249 glucose phase, while the gene expression is relatively unchanged during ethanol phase,
250 see Figure 2B. On the other hand, the gene deletion seems to have affected metabolite
251 expression during both phases, see Figure 2B. Furthermore, in the reference strain, we
252 found that *YGR067C* was significantly under expressed during the ethanol phase
253 compared to the glucose phase (FDR = 4.71x10⁻³³, log2-fold change = 2.05, Wald test
254 with Benjamini-Hochberg (BH) correction), see Supplementary Table 2.1.

255 There were some notable differences in the intracellular metabolism that occurred
256 outside the scope of the original hypothesis, see Table 4. Increased accumulation of

257 riboflavin, glutamic acid and asparagine was observed during both phases in the
 258 deletion mutant. Amino acid expression was mixed during the ethanol phase—
 259 accumulation of glutamic acid, asparagine, and tryptophan were increased in the
 260 mutant while aspartate and phenylalanine abundances had decreased.

261 **Table 4. Statistically different metabolite abundances between the deletion strain and reference strain in each**
 262 **phase (p < 0.1, linear model)**. The metabolites were filtered by the list of compounds found in the yeast9 model.

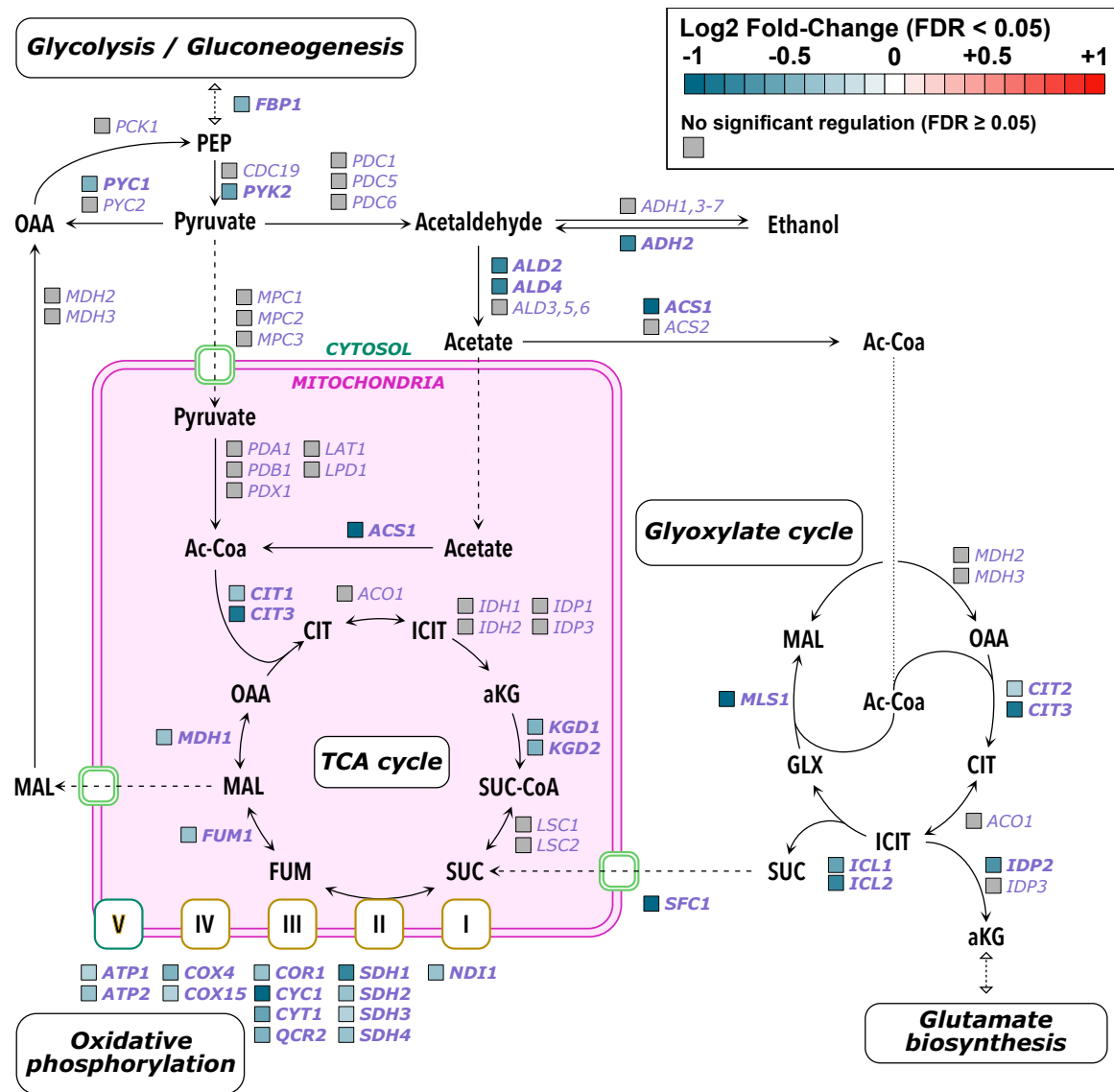
	Query	KEGG	m/z similarity	l2fc	p
Glucose phase	(-)Riboflavin	C00255	0.99	0.60	0.021
	3',5'-Cyclic AMP	C00575	1	2.94	0.042
	Asparagine	C00152	0.98	1.17	0.083
	Glutamic acid	C00025	0.97	0.87	0.020
	L-Carnosine	C00386	0.85	0.43	0.096
	Phosphoenolpyruvic acid	C00074	0.93	-0.08	0.077
Ethanol phase	(-)Riboflavin	C00255	0.99	0.41	0.007
	Asparagine	C00152	0.98	0.77	0.085
	Aspartic acid	C00049	1	-0.74	0.090
	Cytidine 5'-diphosphocholine	C00307	1	1.54	0.025
	Glutamic acid	C00025	0.97	1.74	0.008
	Guanine	C00242	0.94	-0.43	0.089
	NAD+	C00003	0.81	2.82	0.024
	NADH	C00004	0.89	2.82	0.000
	NADP+	C00006	1	3.96	0.039
	O-Phosphoethanolamine	C00346	1	-3.56	0.001
	Phenylalanine	C00079	0.86	-1.06	0.057
	Taurocholate	C05122	0.99	1.36	0.078
	Tryptophan	C00078	1	1.48	0.056

263

264 To investigate whether pathways outside of the main hypothesis were statistically
 265 enriched, topological pathway enrichment was performed on the significantly
 266 differentially expressed genes (FDR < 0.05, Wald test with BH correction) and
 267 metabolites (p-value < 0.1, linear model). Topological pathway enrichment of the gene
 268 expression was performed using pathfindR and only on the DEGs found during the
 269 glucose phase as the number of DEGs during the ethanol phase was too small. The TCA
 270 cycle, glyoxylate pathway, and oxidative phosphorylation, were all downregulated, see
 271 Figure 2D. This was consistent with the hypothesis driven analysis. Furthermore, other
 272 pathways related to carbon utilisation which were not part of the hypothesis were
 273 downregulated, e.g. the carbon metabolism [sce:01200], 2-oxocarboxylic acid
 274 metabolism [sce:01210], and pyruvate metabolism [sce:00620], see Figure 2C.
 275 Ribosome related pathways were significantly upregulated in the *ygr067cΔ* strain,
 276 Ribosome [sce:03010] and Ribosome biogenesis in eukaryotes [sce:03008]. Finally, the

277 pathway Biosynthesis of amino acids [sce:01230] was significantly enriched but did not
278 have a distinct direction of regulation.

279 The topological pathway enrichment of the metabolome was performed using FELLA¹⁹
280 and both glucose- and ethanol phase datasets. During the glucose phase, several
281 signalling pathways were significantly enriched due to the upregulation of 3'-5'-Cyclic
282 AMP [C00575] in the *ygr067cΔ* mutant, see Supplementary Table 5.1. Alanine,
283 aspartate, and glutamate metabolism [sce:00250] and Riboflavin metabolism
284 [sce:00740] were enriched in both phases, most likely due to the increased
285 accumulation of glutamate and asparagine for the prior pathway and increased
286 accumulation of riboflavin for the latter. During the ethanol phase, apart from the
287 previously mentioned pathways, the following pathways were enriched:
288 Glycerophospholipid metabolism [sce:00564], Taurine and hypotaurine metabolism
289 [sce:00430], Ether lipid metabolism [sce:00564], and Nucleotide metabolism
290 [sce:01232] see Figure 2D.



291
292
293
294
295
296

Figure 3. Pathway visualization with transcriptomic regulation of respiratory pathways during the glucose phase. The metabolites are written in black while the genes responsible for the enzymes in the pathway are written in purple. Differentially expressed genes (FDR < 0.05) are written in bold, and the colour of the square represents the log-2 fold change. Genes which were not differentially expressed (FDR ≥ 0.05) are written in plain text and the square is grey. Note that none of the metabolites in this figure were detected in the LCMS.

297

298 Discussion

299 Automation of science is necessary to address the challenges in the quest to fully
300 elucidating the biological function of every gene in *S. cerevisiae*, and other organisms.
301 When automating the scientific cycle, it is necessary to use a model to translate
302 abstract hypotheses into predictable and measurable outcomes. In systems biology the
303 use of mathematical models is particularly important, as each local change (e.g. a gene
304 knockout) will have not only first-order effects on the systems that gene directly
305 interacts with, but higher order effects on other systems in the organism, and these
306 effects are impossible to calculate without a mathematical model. The process of

307 choosing, refining, and applying a model involves taking many decisions. Each of these
308 modelling choices can have a large effect on the predictions, and thus on the evaluation
309 of the hypothesis. To fully automate the scientific cycle, the hypothesis instantiation
310 process must be formalised and recorded.

311 We hypothesised that *YGR067C* induced respiratory pathways during the diauxic shift
312 based on evidence from previous studies. Pathway set prediction (first-order effects)
313 and model-based approaches such as LGEM⁺ and FBA (higher-order effects)
314 transformed this hypothesis into predictions of differential expression of genes and
315 metabolites. Based on the pathway set prediction it was postulated that a
316 downregulation of respiratory genes and decreased abundances of respiratory
317 metabolites would be observed in the *YGR067C* deletion mutant. The LGEM⁺
318 simulations also predicted downregulation in respiratory pathways. The FBA
319 simulations predicted a wider effect on metabolism, including: disruption to
320 fermentation pathways during the glucose phase; and down-regulation of various
321 amino acid and nucleotide biosynthesis pathways, and up-regulation of the glyoxylate
322 cycle during the ethanol phase.

323 The success of a model-driven approach to hypothesis instantiation is dependent on
324 the quality of the model used. Each of the three simulation methods resulted in
325 different predictions, and neither of the model-based predictions worked exceptionally
326 well. LGEM⁺ being a discrete model predicted less disruption than the FBA simulations.
327 A significant modelling challenge was how to translate the abstract hypothesis into the
328 simulation. The technique we used in this study to remove subsets of reactions was
329 chosen because these models only contain metabolic genes and reactions. The low
330 predictive accuracy of both models using this random gene removal indicates this
331 technique needs refinement. A hybrid model, that had representations of signalling and
332 gene regulation connected to the metabolic component, could instantiate the
333 hypothesis differently. Since we hypothesise *YGR067C* to be a transcription factor,
334 developing and implementing a hybrid or whole-cell model, such as that proposed in¹⁶,
335 and instantiating the hypothesis in the gene regulation part of a simulation would be
336 closer to our hypothesis.

337 Another challenge in the modelling is how to predict metabolite accumulation and
338 transcript levels. Both the LGEM⁺ and FBA models are qualitative in their predictions,
339 and we arrived at a prediction of up- or down-regulation by averaging over repeated
340 simulations. It would be more desirable to have a model that predicted transcript levels
341 and metabolite accumulation quantitatively. This is the subject of active research. One
342 recent approach that might be worth future investigation is to use a deep-learning
343 model to predict accumulation from flux²¹.

344 Pathway set hypothesis testing showed that the TCA cycle, oxidative phosphorylation,
345 glyoxylate cycle were statistically enriched during the glucose phase ($p < 0.05$ FGSEA,

346 Fisher's test, and Boschloo's test) and were furthermore distinctly down regulated ($p <$
347 0.05 FGSEA), see Table 1. However, transcription of genes responsible for reactions
348 directing flux from pyruvate to either the TCA cycle or ethanol production were not
349 significantly expressed, see Figure 3. Instead, genes responsible for irreversible steps in
350 the conversion of ethanol to acetyl-Coa, glyoxylate, TCA cycle, and gluconeogenesis
351 were significantly downregulated, see Figure 3. Furthermore, many of the
352 downregulated genes were either glucose repressed (e.g. *PYK2*, *ADH2*, *CIT1*, etc)¹⁵ or
353 induced during consumption of ethanol (*ALD5*, *ALD6*, *PYC1*, etc)²². The evidence from
354 this study therefore suggests that it is more likely that *YGR067C* regulates respiratory
355 genes responsible for flux from ethanol rather from glucose, which passes through
356 pyruvate.

357 There were second-order metabolomic evidence that the glycolytic flux is upregulated
358 in the *ygr067cΔ* strain during the glucose phase. Fermentative glycolysis produces
359 organic acids, such as acetic acid, which acidifies the medium and the cytosol²³. The
360 pH homeostasis is then maintained through V-ATPase-mediated vacuolar
361 acidification²⁴. Two subunits of the V-ATPase complex were upregulated in the deletion
362 mutant, which could be an indication towards increased glycolytic flux. Furthermore,
363 metabolomic analysis showed that 3'-5' cyclic AMP (cAMP) was significantly
364 upregulated in the glucose phase (p -value < 0.1, linear model). cAMP is a crucial
365 signalling metabolite in the Ras/cAMP-pathway that activates protein kinase A, which in
366 turn regulate many processes related to cell growth, such as the diauxic shift²⁵. The
367 Ras/cAMP-pathway is activated by intermediate metabolites in the glycolysis, and the
368 increased cAMP levels could thus be due to the increased glycolytic flux in the deletion
369 mutant²⁴.

370 While respiratory genes were downregulated in the glucose phase, there was no
371 apparent transcriptomic regulation in the ethanol phase. Interestingly however, a
372 significant increase in accumulation of NAD+, NADH, and NADPH was observed in the
373 ethanol phase. Moreover, tryptophan, the precursor molecule for *de novo* NAD
374 synthesis²⁶, showed increased accumulation while phenylalanine, which like
375 tryptophan requires chorismite as a precursor²⁷, saw decreased accumulation. While
376 the relation between the NADH/NAD+ ratio and fermentation, respiration, and aging
377 have been extensively studied²⁸, there does not appear to be much research on
378 increased accumulation of NAD and its derivatives. It is therefore difficult to explain the
379 mechanism behind the NAD+/NADH/NADP+ accumulation based on knowledge from
380 previous studies. One possible explanation would be if the *ygr067cΔ* strains had a less
381 developed mitochondria prior to the diauxic shift and was rapidly producing
382 mitochondrial proteins as glucose was depleted. The increased NAD levels could then
383 be explained by the requirement of NADP(H) during amino acid synthesis, and it would
384 also explain the increased levels of glutamate in the deletion mutant.

385 We found that our hypothesis regarding the role of the uncharacterised ORF *YGR067C*
386 was accurate at a high level, but not specific enough about the predicted effects. The
387 sub-hypothesis, “*YGR067C* induces *ethanol consuming* respiratory pathways *prior to*
388 the diauxic shift” was consistent with the evidence. This lack of specificity in the initial
389 hypothesis has effects on the simulation-based predictions. The accuracy of the
390 simulation-based predictions might have been improved if we had exclusively targeted
391 reactions related to ethanol consumption or had separated the hypothesis into smaller
392 sub-hypotheses, e.g. induction of glucose consuming genes versus induction of ethanol
393 consuming genes.

394 To conclude, we demonstrate several methods to instantiate hypotheses of
395 uncharacterised genes starting from limited knowledge. The performance of the model-
396 driven approaches showed that the techniques and models require more refinement,
397 which we believe is a worthwhile investment for the future of the field. Finally, based on
398 the results of this study, we suggest that previously uncharacterised ORF *YGR067C*
399 induces ethanol consuming respiratory pathways prior to the diauxic shift.

400

401 Methods and materials

402 Pathway set prediction

403 The hypothesis stated that the transcription of genes and the metabolism in pathways
404 associated with respiration would be disrupted in the absence of *YGR067C*. In the
405 pathway set prediction approach, the hypothesis was instantiated by selecting KEGG
406 pathways that were predicted to be differentially expressed between fermentation and
407 respiration: the citric acid cycle (sce00020), oxidative phosphorylation (sce00190),
408 Glyoxylate and dicarboxylate metabolism (sce00630), ethanol synthesis from pyruvate
409 (part of sce00010), genes exclusively expressed during gluconeogenesis (part of
410 sce00010), the pyruvate dehydrogenase complex (part of sce00010), and mitochondrial
411 pyruvate carriers (*MPC1*, *MPC2*, and *MPC3*). Consensus set enrichment, using Fisher’s
412 test, Boschloo’s test, and Fast Gene Set Enrichment Analysis was then performed
413 FGSEA^{29,30}. Fisher’s exact test and Boschloo’s test tends to be overly conservative while
414 FGSEA produces excessive false positives at times^{31,32}. Thus, the methods were chosen
415 to provide a balanced the biological interpretation. The consensus set enrichment was
416 then performed on complete KEGG pathways (sce00020, sce00190, and sce00630)
417 using the predicted gene- and metabolite sets against the empirical transcriptomics
418 and metabolomics data, respectively. The cut-off for the enrichment methods were set
419 to $\alpha = 0.05$. Individual gene- or metabolite regulation was considered when assessing
420 partial pathway predictions.

421

422 **Simulation using LGEM⁺**

423 Metabolic networks can be described in a graph structure which can then be expressed
424 in mathematical logic. Using automated theorem provers we can conduct simulations
425 through logical deduction, and theory repair (hypothesis generation) through
426 abduction³. We constructed a first-order logic model of yeast metabolism based on the
427 consensus genome-scale metabolic model Yeast9 (yeastGEM v9.0.2). This model takes
428 as input a given set of available compounds (in this case the minimal growth medium
429 used for the empirical study), and a goal in the form of a subset of metabolites (the
430 production of a set of compounds deemed essential for yeast to grow). Predictions are
431 logical proofs which correspond to activated reactions, metabolites, and genes. As
432 genome-scale models do not inherently model concentration, those compounds and
433 genes that are included in the LGEM⁺ simulation are those predicted to be present. The
434 simulations are not quantitative, so presence is binary.

435

436 **Simulation using flux balance analysis**

437 To conduct flux balance analysis simulations, we used the Python library CobraPy
438 (version 0.26.3) with the same version of yeastGEM we used to build the LGEM⁺ model
439 (yeastGEM v9.0.2). The default configuration is for growth in a glucose-rich medium and
440 we used this configuration for the simulations for the glucose phase. For the ethanol
441 phase, we set the bounds for glucose exchange to zero and set the ethanol exchange to
442 be 1.0. We used the default growth objective defined in yeastGEM. To obtain predictions
443 for compounds and genes that are expressed, we took the metabolites and genes
444 associated with each reaction that had a flux greater than a stated threshold
445 (1×10^{-9} mmol g⁻¹ DWh⁻¹) in the found solution. Similarly to LGEM⁺, presence for
446 each simulation is therefore binary.

447

448 **Metabolism disruption simulation**

449 YGR067C is not present in Yeast9 v9.0.2 which means that simulating the effect of its
450 deletion from the genome is not directly possible with any computational model built
451 upon Yeast9. We also want to avoid using the empirical transcriptomic data to constrain
452 the simulations, as this would introduce a bias in the simulation, we then want to
453 compare our predictions with the empirical data. So, we need another method of
454 introducing the effect of the deletion into the simulation.

455 In an initial naïve approach, we looked at the compounds and genes in the pathways
456 associated with respiration. For the LGEM⁺ and FBA simulations, we take these same
457 pathways and randomly remove a subset of them before running a growth simulation.
458 This method aims to model the biological effect of a disruption to respiratory pathways,

459 which we hypothesise would be the impact of *YGR067C* deletion. (Note that this
460 method assumes deletion of *YGR067C* would have a negative impact on the respiratory
461 pathways in yeast during the diauxic shift; simulation of a positive regulation after
462 deletion would require a different approach.)

463 This random deletion is repeated N_{sim} times, each time removing a subset of reactions
464 of random size between R_{del}^- and R_{del}^+ . Each simulation results in a prediction of the
465 reactions, metabolites, and genes that are activated, see Table 3. We then calculate the
466 difference between the simulation and the non-disrupted pathway.

467 **Table 3:** Parameters used in the metabolism disruption simulations. * - minimum and maximum number of reactions
468 were found by testing the tolerance of the models to random perturbation, so that the perturbation has a measurable
469 effect on the simulation but does not result in non-growth.

Parameter	Description	Value used	Comment
N_{sim}	Number of simulations conducted	500	
R_{del}^-	Minimum number of reactions removed during disruption simulation	5	Found after testing*
R_{del}^+	Maximum number of reactions removed during disruption simulation	12	Found after testing*

470
471 Each of these simulations results in a slightly different prediction for the metabolic and
472 transcriptomic activity. Our simulation results are stochastic by nature, the randomness
473 introduced in the size and location of the disruption applied to the model.

474 The empirical data from growth experiments also have stochasticity. In this case, the
475 randomness arises from many different sources but will vary across cells within the
476 culture. When measuring growth, transcriptomics, and metabolomics, we are
477 measuring the sum of effects of *YGR067C* deletion across all individual cells,
478 smoothing out this stochasticity.

479 We also sum across our simulations to arrive at data that can be compared to the
480 empirical data, see Figure 1.

481
482

Strain selection and cultivation conditions

483 The *S. cerevisiae* wildtype strain BY4741 (Accession number: Y00000) and single-gene
484 deletion strain BY4741 *YGR067C::kanMX4* (Y04697) were taken from the EUROSCARF
485 deletant library³³. The strains were revived from -80°C glycerol stocks by cultivating
486 them overnight in YPD (2% (w/v) dextrose) media at 30°C, 220 rpm. The strains were
487 then streaked on YPD plates and incubated at 30 ° C for 3 days. Single colonies were
488 then used to inoculate precultures containing YPD (2% (w/v) dextrose) for 15 h at 30°C,
489 220 rpm. Finally, the main cultivations were performed in Thermo Fisher 384 well
490 MATRIX plates (Thermo 4332), with a working volume of 80 µL YNB medium (10.5 g/L
491 YNB without amino acids, 1.25 g/L glucose, 75 µg/L ampicillin, and 0.625 g/L of L-

492 methionine, L-leucine, L-histidine, and Uracil respectively (Brunnsåker et al., 2023).
493 Each culture was inoculated with an initial OD600 of 0.05, and subsequently incubated
494 at 30°C. Every 20 minutes, the well plate was removed from the incubator, agitated
495 using an orbital shaker, aerated by removing the plate lid, and the OD550 was measured
496 using a plate reader (Polarstar). RNAseq and metabolite samples were taken twice,
497 once 12 hours after inoculation, and again after 24 hours.

498 Multiomic extraction and processing

499 Current RNA extraction protocols and LCMS protocols require biomass concentrations
500 which are not feasible with 80 µL cultures. 96 wells were therefore pooled into one
501 biological replicate for the RNA and metabolite extraction protocols using the liquid
502 handler Bravo. The pooled cell broth meant for RNA extraction was then centrifuged
503 (5,000 rcf, 5 min) and the RNA was immediately extracted using RNeasy kits (QIAGEN).
504 The extracted RNA was stored in 30 µL RNase free water at -80°C. Total RNA quantity
505 and quality was measured using BioAnalyzer. The library construction and sequencing
506 were performed by Azenta in Leipzig, Germany. Data are deposited at European
507 Nucleotide Archive (PRJEB60302). The raw .fastq files were processed using the nf-
508 core/rnaseq v3.10.1 pipeline³⁴, using the *S. cerevisiae* reference genome Ensembl entry
509 R64-1-1, STAR³⁵ for fragment alignment and Salmon³⁶ for quantification.

510 The extraction protocol is described in a previous study⁷. Untargeted metabolomics
511 profiling was performed on a Waters Xevo G2-sX qTOF high-resolution mass
512 spectrometers (HRMS) coupled to a Waters Acquity Classic UPLC instrument.
513 Metabolites were separated on an UPLC HSS T3 (1.8 µm, 2.1 × 100 mm, Waters) column
514 with a water-MeOH gradient solvent system containing 0.04% formic acid. The gradient
515 started at 5% MeOH with formic acid (MPB) and ramped to 100% MPB over 6 min and
516 held for 4.50 min at 100% MPB. Column temperature was set to 45 °C and the flow at
517 0.4 mL/min. Mass spectra was acquired using an electrospray ionization (ESI) source in
518 either positive or negative ionization mode scanning from 40 to 1200 m/z at 5
519 spectra/second. The capillary voltage was set at 1500 V (ESI negative) and 2000 V (ESI
520 positive), and cone voltage at 40. The source temperature was set at 120°C, desolvation
521 a gas temperature at 600°C, desolvation and cone gas flow at 700 and 10 L/min,
522 respectively. Data-dependent MS2 data was collected in both positive and negative
523 ionization by using the following parameters: mass range 40-1200 m/z, MS survey
524 switching threshold 5000, MS survey scanning 0.2 sec, maximum number of precursors
525 6, scan rate for MS/MS 0.1 sec, collision energy ramp LM CE ramp 6-9 to 60-80 over a
526 mass range of 40-1200 m/z. The raw mass spectra were converted into .mzML files using
527 ProteWizard's msConvert³⁷. Peak picking and initial processing were performed using
528 MSDIAL (v5.4)³⁸. Identification was performed using the Riken library of both positive
529 and negative ion mode³⁸. The identified peaks were then processed using the Notame³⁹
530 pipeline in R (v. 4.5.0).

531

532 **Statistical analysis of empirical data**

533 The phenomic analysis was performed by first compiling the recorded measurements
534 from OMEGA into a .csv file. The .csv file was then used to generate input files
535 compatible for AMiGA⁴⁰. AMiGA then calculates $\ln(\text{OD}_{560})$ and $d/dt \ln(\text{OD}_{560})$ at each
536 timepoint t. The carrying capacity $\text{OD}_{560, \text{max}}$ is obtained by finding the maximum value of
537 $\ln(\text{OD}_{560})$ during the experiment while the maximum biomass specific growth rate, μ ,
538 was obtained by finding the maximum of $d/dt \ln(\text{OD}_{560})$. Since we did not know the
539 distribution of the biomass specific growth rate and maximum OD_{560} , the statistical
540 difference between the reference strain and mutant strain were assessed by performing
541 a permutation test, which is a non-parametric test. The observed test statistic, T_{obs} ,
542 was calculated by taking the difference in median response value between the strains.
543 The null distribution was then generated by resampling the growth parameter data and
544 recalculating the test statistic n = 10,000 times. The two-sided p-value was then
545 calculated by counting how many times 1 + the absolute value of the sampled
546 permutations exceeded the absolute value of the observed test statistic, divided by n.

547 The transcriptomics analysis was performed using the DESeq2 software package⁴¹. Raw
548 expression data, see Supplementary Table 2.1, were normalised, fit to a negative
549 binomial distribution, and the log2-fold change of low expression genes was adjusted
550 using the DESeq2-package in R. Hypothesis testing was performed using the Wald test
551 and were corrected for false positives using FDR/Benjamini-Hochberg method with a
552 cut-off of FDR < 0.05. The following contrasts were used for this study: *ygr067cΔ* versus
553 reference during glucose phase, *ygr067cΔ* versus reference during ethanol phase. The
554 log2-fold changes (Log2FC) were shrunk using DESeq2's lfcShrink function with the
555 'ashr' setting⁴².

556 The metabolomics analysis was performed using the notame package³⁹. Univariate
557 significance testing of the identified peaks was performed using linear modelling. The
558 signal intensity was set as the dependent variable while the group (*ygr067cΔ* mutant
559 versus reference) was the independent variable. The p-value cut-off was set to p-value <
560 0.1, similar to previous studies⁴³.

561 Topological enrichment analysis was performed using active-subnetwork-oriented
562 enrichment analysis through the pathfindR package for the transcriptomic data. For the
563 metabolomics datam, a diffusion based method was performed using FELLA¹⁹. The
564 protein-protein interaction network used in both topological enrichment analysis were
565 constructed using KEGG graph objects downloaded from KEGG (date). Topological
566 pathway enrichment was performed on the significantly differentially expressed genes
567 (FDR < 0.05, Wald test with BH correction) and metabolites (p-value < 0.1, linear
568 model).

569

570 Data availability

571 Data deposition: RNA-seq data has been submitted in the form of raw reads in the form
572 of .fastq files under the accession number PRJEB60302 at the European Nucleotide
573 Archive (ENA). Metabolomics data has been submitted in the form of derived spectral
574 .mzML files under the accession number MTBLS12663 at the Metabolights.

575

576 Code availability

577 All code required for reproduction of the analysis and figures in the study can be found
578 on GitHub at https://www.github.com/erikbju/YGR067C_Dshift.

579

580 References

- 581 1. Wood, V. et al. Hidden in plain sight: what remains to be discovered in the eukaryotic
582 proteome? *Open Biol.* **9**, 180241 (2019).
- 583 2. Sordo Vieira, L. & Laubenbacher, R. C. Computational models in systems biology:
584 standards, dissemination, and best practices. *Current Opinion in Biotechnology* **75**,
585 102702 (2022).
- 586 3. Gower, A. H., Korovin, K., Brunnsåker, D., Tiukova, I. A. & King, R. D. LGEM+: A First-
587 Order Logic Framework for Automated Improvement of Metabolic Network Models
588 Through Abduction. in *Discovery Science* (eds Bifet, A., Lorena, A. C., Ribeiro, R. P.,
589 Gama, J. & Abreu, P. H.) vol. 14276 628–643 (Springer Nature Switzerland, Cham,
590 2023).
- 591 4. Murphy, J. P., Stepanova, E., Everley, R. A., Paulo, J. A. & Gygi, S. P. Comprehensive
592 Temporal Protein Dynamics during the Diauxic Shift in *Saccharomyces cerevisiae*.
593 *Molecular & Cellular Proteomics* **14**, 2454–2465 (2015).

- 594 5. Schlossarek, D. *et al.* Rewiring of the protein–protein–metabolite interactome during
595 the diauxic shift in yeast. *Cell. Mol. Life Sci.* **79**, 550 (2022).
- 596 6. Brauer, M. J., Saldanha, A. J., Dolinski, K. & Botstein, D. Homeostatic adjustment and
597 metabolic remodeling in glucose-limited yeast cultures. *Mol Biol Cell* **16**, 2503–2517
598 (2005).
- 599 7. Brunnsåker, D. *et al.* High-throughput metabolomics for the design and validation of a
600 diauxic shift model. *npj Syst Biol Appl* **9**, 11 (2023).
- 601 8. King, R. D. *et al.* The Automation of Science. *Science* **324**, 85–89 (2009).
- 602 9. Roper, K. *et al.* Testing the reproducibility and robustness of the cancer biology
603 literature by robot. *J. R. Soc. Interface* **19**, 20210821 (2022).
- 604 10. Sigurdardóttir, S. *et al.* An automated positive selection screen in yeast provides
605 support for boron-containing compounds as inhibitors of SARS-CoV-2 main
606 protease. *Microbiol Spectr* **12**, e01249-24 (2024).
- 607 11. Williams, K. *et al.* Cheaper faster drug development validated by the repositioning of
608 drugs against neglected tropical diseases. *J. R. Soc. Interface* **12**, 20141289 (2015).
- 609 12. Böhm, S., Frishman, D. & Mewes, H. W. Variations of the C2H2 zinc finger motif in
610 the yeast genome and classification of yeast zinc finger proteins. *Nucleic Acids Res*
611 **25**, 2464–2469 (1997).
- 612 13. Young, E. T., Dombek, K. M., Tachibana, C. & Ideker, T. Multiple Pathways Are Co-
613 regulated by the Protein Kinase Snf1 and the Transcription Factors Adr1 and Cat8.
614 *Journal of Biological Chemistry* **278**, 26146–26158 (2003).
- 615 14. De Deken, R. H. The Crabtree Effect: A Regulatory System in Yeast. *Journal of*
616 *General Microbiology* **44**, 149–156 (1966).

- 617 15. Kayikci, Ö. & Nielsen, J. Glucose repression in *Saccharomyces cerevisiae*. *FEMS*
618 *Yeast Research* **15**, fov068 (2015).
- 619 16. Espinosa, M. I. *et al.* Adaptive laboratory evolution of native methanol assimilation
620 in *Saccharomyces cerevisiae*. *Nat Commun* **11**, 5564 (2020).
- 621 17. Rathod, R., Gajera, B., Nazir, K., Wallenius, J. & Velagapudi, V. Simultaneous
622 Measurement of Tricarboxylic Acid Cycle Intermediates in Different Biological
623 Matrices Using Liquid Chromatography–Tandem Mass Spectrometry; Quantitation
624 and Comparison of TCA Cycle Intermediates in Human Serum, Plasma, Kasumi-1
625 Cell and Murine Liver Tissue. *Metabolites* **10**, 103 (2020).
- 626 18. Di Bartolomeo, F. *et al.* Absolute yeast mitochondrial proteome quantification
627 reveals trade-off between biosynthesis and energy generation during diauxic shift.
628 *Proc. Natl. Acad. Sci. U.S.A.* **117**, 7524–7535 (2020).
- 629 19. Picart-Armada, S., Fernández-Albert, F., Vinaixa, M., Yanes, O. & Perera-Lluna, A.
630 FELLA: an R package to enrich metabolomics data. *BMC Bioinformatics* **19**, 538
631 (2018).
- 632 20. Lu, H., Kerkhoven, E. J. & Nielsen, J. Multiscale models quantifying yeast physiology:
633 towards a whole-cell model. *Trends in Biotechnology* **40**, 291–305 (2022).
- 634 21. Morrissey, J., Barberi, G., Strain, B., Facco, P. & Kontoravdi, C. NEXT-FBA: A hybrid
635 stoichiometric/data-driven approach to improve intracellular flux predictions.
636 *Metabolic Engineering* **91**, 130–144 (2025).
- 637 22. Brewster, N. K., Val, D. L., Walker, M. E. & Wallace, J. C. Regulation of pyruvate
638 carboxylase isozyme (PYC1, PYC2) gene expression in *Saccharomyces cerevisiae*
639 during fermentative and nonfermentative growth. *Arch Biochem Biophys* **311**, 62–71
640 (1994).

- 641 23. Casal, M., Cardoso, H. & Leao, C. Mechanisms regulating the transport of acetic
642 acid in *Saccharomyces cerevisiae*. *Microbiology* **142**, 1385–1390 (1996).
- 643 24. Deprez, M.-A., Eskes, E., Wilms, T., Ludovico, P. & Winderickx, J. pH homeostasis
644 links the nutrient sensing PKA/TORC1/Sch9 ménage-à-trois to stress tolerance and
645 longevity. *Microb Cell* **5**, 119–136 (2018).
- 646 25. Thevelein, J. M. & De Winde, J. H. Novel sensing mechanisms and targets for the
647 cAMP–protein kinase A pathway in the yeast *Saccharomyces cerevisiae*. *Molecular*
648 *Microbiology* **33**, 904–918 (1999).
- 649 26. Savitz, J. The kynurenine pathway: a finger in every pie. *Mol Psychiatry* **25**, 131–147
650 (2020).
- 651 27. Braus, G. H. Aromatic amino acid biosynthesis in the yeast *Saccharomyces*
652 *cerevisiae*: a model system for the regulation of a eukaryotic biosynthetic pathway.
653 *Microbiol Rev* **55**, 349–370 (1991).
- 654 28. Odoh, C. K., Guo, X., Arnone, J. T., Wang, X. & Zhao, Z. K. The role of NAD and NAD
655 precursors on longevity and lifespan modulation in the budding yeast,
656 *Saccharomyces cerevisiae*. *Biogerontology* **23**, 169–199 (2022).
- 657 29. Subramanian, A. *et al.* Gene set enrichment analysis: A knowledge-based approach
658 for interpreting genome-wide expression profiles. *Proc. Natl. Acad. Sci. U.S.A.* **102**,
659 15545–15550 (2005).
- 660 30. Boschloo, R. D. Raised conditional level of significance for the 2 × 2-table when
661 testing the equality of two probabilities. *Statistica Neerlandica* **24**, 1–9 (1970).
- 662 31. Abatangelo, L. *et al.* Comparative study of gene set enrichment methods. *BMC*
663 *Bioinformatics* **10**, 275 (2009).

- 664 32. Dinu, I. *et al.* Improving gene set analysis of microarray data by SAM-GS. *BMC*
665 *Bioinformatics* **8**, 242 (2007).
- 666 33. Giaever, G. & Nislow, C. The Yeast Deletion Collection: A Decade of Functional
667 Genomics. *Genetics* **197**, 451–465 (2014).
- 668 34. Harshil Patel *et al.* nf-core/rnaseq: nf-core/rnaseq v3.10.1 - Plastered Rhodium
669 Rudolph. Zenodo <https://doi.org/10.5281/ZENODO.7505987> (2023).
- 670 35. Dobin, A. *et al.* STAR: ultrafast universal RNA-seq aligner. *Bioinformatics* **29**, 15–21
671 (2013).
- 672 36. Patro, R., Duggal, G., Love, M. I., Irizarry, R. A. & Kingsford, C. Salmon provides fast
673 and bias-aware quantification of transcript expression. *Nat Methods* **14**, 417–419
674 (2017).
- 675 37. Adusumilli, R. & Mallick, P. Data Conversion with ProteoWizard msConvert. in
676 *Proteomics* (eds Comai, L., Katz, J. E. & Mallick, P.) vol. 1550 339–368 (Springer New
677 York, New York, NY, 2017).
- 678 38. Tsugawa, H. *et al.* MS-DIAL: data-independent MS/MS deconvolution for
679 comprehensive metabolome analysis. *Nat Methods* **12**, 523–526 (2015).
- 680 39. Klåvus, A. *et al.* “Notame”: Workflow for Non-Targeted LC–MS Metabolic Profiling.
681 (2020).
- 682 40. Midani, F. S., Collins, J. & Britton, R. A. AMiGA: Software for Automated Analysis of
683 Microbial Growth Assays. *mSystems* **6**, 10.1128/msystems.00508-21 (2021).
- 684 41. Love, M. I., Huber, W. & Anders, S. Moderated estimation of fold change and
685 dispersion for RNA-seq data with DESeq2. *Genome Biol* **15**, 550 (2014).
- 686 42. Stephens, M. False discovery rates: a new deal. *Biostat* kxw041 (2016)
687 doi:10.1093/biostatistics/kxw041.

688 43. Raguz Nakic, Z., Seisenbacher, G., Posas, F. & Sauer, U. Untargeted metabolomics
689 unravels functionalities of phosphorylation sites in *Saccharomyces cerevisiae*. *BMC*
690 *Syst Biol* **10**, 104 (2016).

691

692

693 Acknowledgements

694 *This work was partially supported by the Wallenberg AI, Autonomous Systems and*
695 *Software Program (WASP) funded by Knut and Alice Wallenberg foundation and the*
696 *Swedish Research Council Formas (grant agreement no. 2020-01690). Funding was*
697 *also provided by the Chalmers AI Research Centre.*

698 *This work has been supported by the UK Engineering and Physical Sciences Research*
699 *Council (EPSRC) [EP/R022925/2, EP/W004801/1 and EP/X032418/1],*

700 *The computations/data handling were enabled by resources in project NAISS 2023/22-*
701 *185 (computation) and NAISS 2023/23-80 (data storage) provided by the National*
702 *Academic Infrastructure for Supercomputing in Sweden (NAISS) at UPPMAX, funded by*
703 *the Swedish Research Council (grant agreement no. 2022-06725).*

704

705 Author Contributions

706 Conceptualisation and design of study: E.Y.B., I.A.T, and R.D.K. Hypothesis instantiation
707 and simulation: A.H.G. Cultivation experiment: E.Y.B., A.H.G., and P.L. Multiomics
708 extraction: P.L. and E.Y.B. LC/MS processing: O.I.S. Data analysis: E.Y.B. and A.H.G.
709 Writing: E.Y.B., A.H.G., O.I.S, I.A.T., and R.D.K. All authors read and approved the final
710 manuscript.

711

712 Funding

713 Open access funding provided by Chalmers University of Technology.

714

715 Competing Interests

716 The authors declare no competing interests.

717

718 **Ethics Approval and Consent to Participate**

719 The authors declare no competing interests.

720

721 **Supplementary material**

722 S. Table 1 – Log-files for growth curves obtained using omega polarstar

723 S. Table 2.1 – Normalized transcript counts

724 S. Table 2.2 – Differential expression tables of RNAseq data

725 S. Table 3.1 – Aligned metabolite data

726 S. Table 3.2 – Differential expression tables of Metabolite data

727 S. Table 4.1 – Pathway set prediction

728 S. Table 4.2 – Simulated prediction

729 S. Table 5.1 – Topological enrichment, metabolomics